Numerical simulation of surface energy and water balances over a semiarid grassland ecosystem in the West African Savanna

Emmanuel Quansah, Genki Katata, Matthias Mauder, Thompson Annor, Leonard K. Amekudzi, Jan Bliefernicht, Dominikus Heinzeller, Ahmed A. Balogun, Harald Kunstmann

Research Article

Numerical Simulation of Surface Energy and Water Balances over a Semiarid Grassland Ecosystem in the West African Savanna

Emmanuel Quansah,[1] Genki Katata,[2] Matthias Mauder,[3] Thompson Annor,[1] Leonard K. Amekudzi,[1] Jan Bliefernicht,[4] Dominikus Heinzeller,[3] Ahmed A. Balogun,[5] and Harald Kunstmann[3,4]

[1]*Meteorology and Climate Science Unit, Department of Physics, Kwame Nkrumah University of Science and Technology, Kumasi, Ghana*
[2]*Japan Atomic Energy Agency, Ibaraki, Japan*
[3]*Institute of Meteorology and Climate Research, Karlsruhe Institute of Technology, Garmisch-Partenkirchen, Germany*
[4]*Chair for Regional Climate and Hydrology, University of Augsburg, Augsburg, Germany*
[5]*Department of Meteorology and Climate Science, Federal University of Technology, Akure, Nigeria*

Correspondence should be addressed to Matthias Mauder; matthias.mauder@kit.edu

To understand surface energy exchange processes over the semiarid regions in West Africa, numerical simulations of surface energy and water balances were carried out using a one-dimensional multilayer atmosphere-SOil-VEGetation (SOLVEG) model for selected days of the dry and rainy seasons over a savanna grassland ecosystem in Sumbrungu in the Upper East region of Ghana. The measured Bowen ratio was used to partition the residual energy into the observed sensible heat flux (H) and latent heat flux (LE) in order to investigate the impact of the surface energy closure on model performance. The results showed that the model overall reproduced the diurnal changes in the observed energy fluxes, especially the net radiation (Rn), compared to half-hourly eddy covariance flux measurements, for the study periods. The performance measure in terms of the correlation coefficient (R), centred root mean square error (RMSE), and normalized standard deviation (σ) between the simulated H and LE and their corresponding uncorrected observed values ranged between $R = 0.63$–0.99 and 0.83–0.94, RMSE $= 0.88$–1.25 and 0.88–1.92, and $\sigma = 0.95$–2.23 and 0.13–2.82 for the dry and rainy periods respectively, indicating a moderate to good model performance. The partitioning of H and LE by SOLVEG was generally in agreement with the observations during the dry period but showed clear discrepancies during the rainy period, particularly after rainfall events. Further sensitivity tests over longer simulation periods (e.g., 1 year) are required to improve model performance and to investigate seasonal exchanges of surface energy fluxes over the West African Savanna ecosystems in more details.

1. Introduction

Land surface models (LSMs) have a role in partitioning the energy influx of net radiation into sensible and latent heat fluxes in atmospheric models [1]. Since these partitioned energy fluxes influence the development of the boundary layer, cloud formation, weather, and climate [2], their accurate representation in LSMs is required for weather and climate simulations [3, 4]. Although several authors have demonstrated the ability of LSMs to partition the surface energy flux over the temperate regions [1, 2, 5, 6], still a few number of LSM studies have been carried out over the semiarid regions in Africa using measurements from eddy covariance stations for model validation [7–9]. For instance, Schüttemeyer [7] and Bagayoko et al. [8] investigated the performance of the Noah-LSM developed by the National Centre for Atmospheric Research, NCAR [10], to simulate the energy fluxes with respect to the seasonal dynamics of

vegetation cover over the Sudanian Savannas of West Africa. The results revealed that the model was able to simulate the surface energy fluxes such as net radiation, sensible heat flux, and latent heat flux during the wet period. However, it was not sensitive to the changes in the roughness length for momentum on both seasonal and daily bases. This fact was attributed to the coefficient that related transpiration and evaporation to the atmosphere [7, 8].

To investigate land-surface atmosphere interactive processes in arid and semiarid terrains, a one-dimensional multilayer atmosphere-SOil-VEGetation (SOLVEG) model was modified to include sophisticated evaporation and water adsorption schemes for dry soil [11, 12]. In contrast to many other land surface models, the schemes for water movements in SOLVEG simulate evaporation even during dry conditions when the soil moisture content reaches the wilting point. The model could therefore be suitable for estimating surface energy and water balances with an interaction of stomatal regulation process under seasonal dynamics of African climate, particularly during the dry period. The model has been successfully validated with data from the Negev desert in Israel [12]. A comparative study had been carried out between SOLVEG and the Noah-LSM to compare their ability to replicate water content, soil temperature and surface fluxes in the Negev Desert during the dry season. The results showed that the modified schemes in SOLVEG for evaporation and adsorption in the soil gave good predictions of the surface fluxes, soil temperature, and soil water content [12]. Recently, a novel meteorological network with Eddy Covariance stations has been established in the West African Savanna [13, 14]. This work therefore provides a unique opportunity to evaluate SOLVEG for the first-time using data from a semiarid test site in West Africa.

The present study therefore aims to apply and evaluate SOLVEG over a grassland ecosystem in the West African Sudanian Savanna. The performance of the model is tested using a dataset of surface energy fluxes and volumetric soil water content for a selected 1 month and 26 days during both the dry and wet periods, respectively, in 2013. In addition, a correction of the latent heat and sensible heat flux measurements is performed to improve the energy imbalance over a grassland ecosystem and to investigate whether this type of correction can improve model simulations.

2. Materials and Methods

2.1. Description of Study Site.
The study site is located in Sumbrungu (10.846°N, 0.917°W, 200 m asl) in the Upper East Region of Ghana (Figure 1). The climate and vegetation of the area is the Southern Sudanian Savanna, with grassland ecosystem interspersed with trees. The dominant grass types include *Brachiaria lata, Chloris piloasa,* and *Cassia mimosoides*, with an average height of 0.10 m at the end of the wet period in October each year. The dominant tree types are *Lannea microcarpa, Adansonia,* and *Parkia biglobosa*, with heights between 3 and 5 m and spacing of 30 to 40 m apart [14]. The dry period is between November and April each year. The annual rainfall is monomodal and starts in May and

ends in October each year. The annual precipitation over the region ranges between 320 and 1100 mm [15–18]. The annual precipitation during the investigated period (2013) from a nearby climate station at Bongo Soe (10.973°N, 0.783°W and 200 m asl) and located at 20 km north-eastern of the study site was 542 mm. The daily mean air temperature for the study area in 2013 ranged between 23.3 and 34.7°C [14].

2.2. Observational Data.
Half-hourly observed sensible heat flux (H) and latent heat flux (LE) for the year 2013 were determined based on the Eddy Covariance (EC) technique according to Quansah et al. [14] and Mauder and Foken [19]:

$$H = \rho_a c_p \overline{w'T_a'}, \tag{1}$$

$$LE = \lambda \overline{w'\rho_v'}, \tag{2}$$

where ρ_a is the density of dry air at a given air temperature ($kg\,m^{-3}$), c_p is the specific heat capacity of dry air at constant pressure ($J\,kg^{-1}\,K^{-1}$), T_a is the air temperature derived from the ultrasonic anemometer (°C), λ is the latent heat of evaporation ($J\,kg^{-1}$), w is the vertical component of the wind velocity ($m\,s^{-1}$), and ρ_v is the molar density of water vapour ($mol\,m^{-3}$). Overbars represent time averages and primes denote fluctuations around these averages. Similarly, half-hourly values of the net radiation and the ground heat flux were determined based on the methods described in Quansah et al. [14]. The selected dry and rainy days used in this study were chosen, because they represented a period of high quality data for model validation. The quality controls of the measurements are based on statistical algorithms described in [19].

Meteorological data of air temperature (°C), surface pressure (hPa), rainfall intensity ($mm\,h^{-1}$), wind speed ($m\,s^{-1}$), wind direction (°), incoming solar radiation ($W\,m^{-2}$), outgoing longwave radiation ($W\,m^{-2}$), specific humidity ($g\,kg^{-1}$), and CO_2 concentration (ppmv) were required as input variables for the model simulations. These data were also obtained from the EC site and were available between January and December 2013. Similarly, values for the initial volumetric soil water content and soil bottom temperature as well as other initial variables required by the model were obtained from the EC site. Table 1 provides a summary of selected devices and their measurement heights at the study site.

2.3. Energy Balance Closure Adjustment.
Half-hourly sensible heat flux (H), latent heat flux (LE), net radiation (Rn), and ground heat flux (G) were observed at the study site [14]. The energy balance closure for both the dry and wet periods were estimated using a linear regression fit between ($Rn - G$) and ($H + LE$). The surface energy fluxes observed using the EC method are often not closed, with a global nonclosure in which the sum of the turbulence fluxes ($H + LE$) has been found to be between 10–30% less than the available energy ($Rn - G$) [20]. This has been attributed to the noncapturing of large-scale transports by regular EC tower measurements and errors in measurements from individual instrument [2, 20].

TABLE 1: Summary of measurement heights of selected data used for SOLVEG simulations.

| Variable	Device/manufacturer	Measurement height [m]
Atmospheric CO_2 and H_2O	Licor 7500A open path infrared gas analyser, LI-COR Biosciences, USA	2.65
Wind speed in 3-dimensional field (u, v, and w) and air temperature	CSAT3 ultrasonic anemometer, Campbell Scientific, USA	2.65
Incoming and outgoing shortwave and longwave radiations	CNR4 net radiometer (pair of pyranometer and pyrgeometer), Kipp & Zonen, Netherlands	2.00
Soil moisture content	CS616, water content reflectometer, Campbell Scientific, USA	0.03
Soil heat flux	HFP01SC, self-calibrating heat flux plate, Hukseflux, Netherlands	0.08
Soil temperature	TCAV averaging soil thermocouple probe, Campbell Scientific, USA	0.03
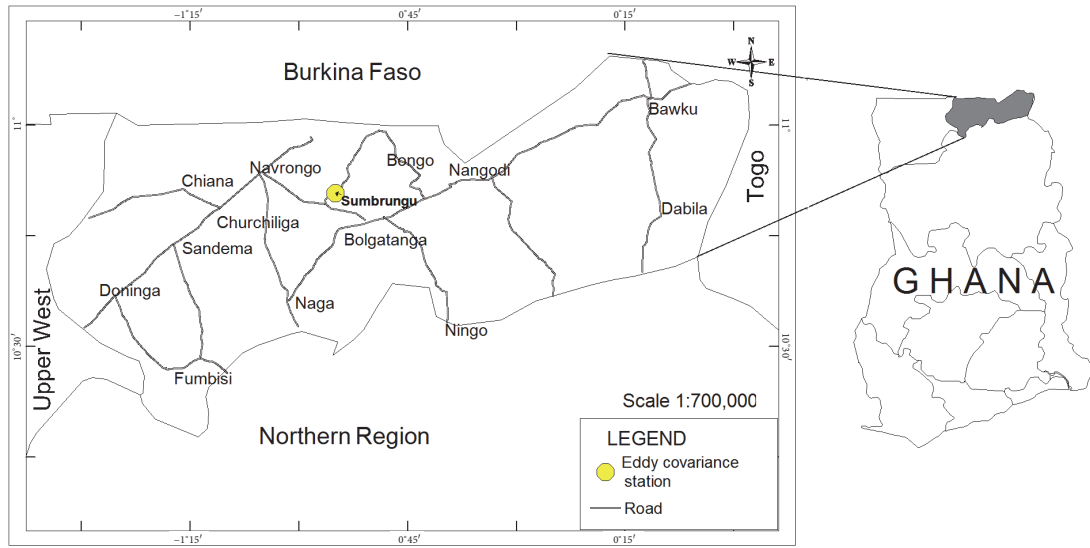
FIGURE 1: The map of the study sites, including the location of the Eddy Covariance station.

Nevertheless, this energy imbalance can be improved based on the partitioning of the residual energy into H and LE using the measured Bowen ratio, B_o, according to Ingwersen et al. [2] and Twine et al. [21]:

$$B_o = \frac{H}{LE}. \tag{3}$$

This approach using (3) leads to a corrected observed sensible heat flux, H^* (W m^{-2}), and latent heat flux, LE* (W m^{-2}):

$$H^* = Rn - G - LE^*, \tag{4}$$

$$LE^* = \frac{Rn - G}{B_o + 1}. \tag{5}$$

The surface energy balance is usually required when comparing model results with observational data, since the land surface models principally assume the full closure of the energy balance based on vertical exchange processes only.

2.4. Numerical Simulations

2.4.1. Model Overview. In the atmospheric submodule, the turbulent exchange fluxes are solved numerically based on the one-dimensional diffusion equations for the horizontal wind speed components u and v (m s^{-1}), potential temperature θ (K), specific humidity q_a (kg kg^{-1}), liquid water content of fog w_f (kg kg^{-1}), turbulence kinetic energy e (m^2 s^{-2}), turbulence length scale λ_t (m), and CO_2 concentration (ppmv). Using φ as a generalised variable for all components, the one-dimensional diffusion equations are described in the same form as indicated in the following [22]:

$$\frac{\partial \varphi}{\partial t} = \frac{\partial}{\partial z_a} K_z \frac{\partial \varphi}{\partial z_a} + F_\varphi. \tag{6}$$

Here, z_a is the depth within the atmosphere from the surface (m), t is the time interval (s), K_z is the vertical turbulence diffusivity (m^2 s^{-1}), and F_φ is the forcing component that consists of the exchange between the vegetation and canopy air as the volume source or sink for each atmospheric variable

TABLE 2: General parameters used for the SOLVEG simulations.

Parameter	Settings
Calculation period	01 to 31 January (dry period) and 01 to 26 June, 2013 (wet period)
Vegetation type	C4 grass
Atmospheric and vegetation layer in height (m)	0.05, 0.1, 0.2, 0.4, 1.0, 2.0, 4.0, 6.0, 8.0, and 10.0
Soil layer in depth (m)	0.0, 0.05, 0.08, 0.1, 0.2, 0.3, 0.5, 1.0, and 2.0
Initial volumetric soil water content (m^3 m^{-3})	0.017 and 0.03 for the dry and wet periods, respectively

(it assumes the unit of the variable of interest). The radiation energy inputs for the calculation of the energy budget at the layers between the soil and the vegetation canopy are calculated according to schemes that separately consider the direct and diffuse downward and upward fluxes of solar radiation in the canopy.

In the soil submodule, the temporal changes in soil temperatures are calculated based on the heat conduction equation:

$$C_s \rho_s \frac{\partial T_s}{\partial t} = \frac{\partial}{\partial z_s}\left(\mu \frac{\partial T_s}{\partial z_s}\right) - \lambda E_b, \qquad (7)$$

where C_s is the specific heat capacity of bulk soil ($J\,kg^{-1}\,K^{-1}$), ρ_s is the density of the bulk soil ($kg\,m^{-3}$), T_s is the soil temperature (K), t is the time interval (s), z_s is the depth of the soil (m), μ is the thermal conductivity ($W\,m^{-1}\,K^{-1}$), λ is the latent heat of vapourisation ($J\,kg^{-1}$), and E_b is the evaporation or condensation rate of soil moisture ($kg\,m^{-2}\,s^{-1}$). The mass balance equation for liquid water is also expressed as

$$\rho_w \frac{\partial \eta_w}{\partial t} = \left(D_w \frac{\partial \eta_w}{\partial z_s} + K_c\right) - E_b, \qquad (8)$$

where η_w is the volumetric soil water content ($m^3\,m^{-3}$), D_w is the soil water diffusivity ($m^2\,s^{-1}$), K_c is the unsaturated hydraulic conductivity ($m\,s^{-1}$), and ρ_w is the density of liquid water ($kg\,m^{-3}$). The soil water diffusivity D_w is given as

$$D_w = K_c \frac{\partial \psi}{\partial \eta_w}, \qquad (9)$$

where ψ is the soil water potential (m). The Fick's law of diffusion of water vapour in soil pores is employed to describe the water vapour diffusion in the soil:

$$\rho \frac{\partial (\eta_{ws} - \eta_w) q_s}{\partial t} = \frac{\partial}{\partial z_s} \rho \varepsilon_t \left(D_v (\eta_{ws} - \eta_w) \frac{\partial q_s}{\partial z_s}\right) \\ + E_b, \qquad (10)$$

where ρ is the density of water vapour ($kg\,m^{-3}$), η_{ws} is the saturated volumetric water content ($m^3\,m^{-3}$), q_s is the specific humidity in the soil pores ($kg\,kg^{-1}$), D_v is the diffusion coefficient of water vapour ($m^2\,s^{-1}$), and ε_t is the tortuosity. The expression $(\eta_{ws} - \eta_w)$ stands for the volumetric content of gaseous phase in the soil. In the SOLVEG model, ε_t is chosen as two-thirds, according to [23].

The model includes schemes for evaporation and adsorption in the soil to adapt it to arid and semiarid regions. A soil water retention curve of [24], for the capillary region [25] and the adsorption region [26], is used in (9) to simulate the soil water movement from saturated to very dry soil. The module calculates not only surface evaporation of capillary water but also internal evaporation from adsorbed water films on "cylindrical pores" in soil (E_b in (8) and (10)). This enables the model to provide good predictions of surface fluxes and soil temperature and moisture profiles in dry soil [12]. Further details on the performance of SOLVEG to predict heat, water, and CO_2 exchanges at semiarid areas can be found in [12]. Simulation conditions of SOLVEG used in this study have been summarised in Table 2.

2.4.2. Performance Measures. The agreements between the observed and predicted variables were evaluated based on their correlation coefficients (R) and centred root-mean-square differences (RMSE). In addition, the variations of the simulations in comparison to the variations of the observations are evaluated using a normalized standard deviation based on the ratio of the predicted variance to the observed variance [27]. A ratio larger than one indicates an overestimation of the observed variability whereas a ratio smaller than one denotes an underestimation. The calculation of the performance measure was done for each variable, namely, the net radiation (Rn), sensible heat flux (H), latent heat flux (LE), ground heat flux (G), and the volumetric soil moisture content (Sm). Figure 4 shows the statistical values of the simulated H and LE when they are compared with their corresponding observed values without the residual energy corrections, while Hn and LEn denote values of the comparison after the residual energy corrections.

3. Results and Discussion

3.1. Dry Period Simulation. The time series of the simulated and observed net radiation (Rn), sensible heat flux (H), latent heat flux (LE), ground heat flux (G), and volumetric soil moisture content (Sm) for the selected days during the dry period from 1 to 31 January 2013 at the study site are shown in Figure 2. The results show that best matches of the simulated and observed variables are obtained for Rn during the period. The daily maximum values for the simulated parameters are 443, 337, 33, and 55 W m^{-2} for Rn, H, LE, and G, respectively, while the daily maximum values for the observed Rn, H, LE, and G are 422, 257, 49, and 91 W m^{-2}, respectively (Figure 2). The observed soil water content is very low in the dry period
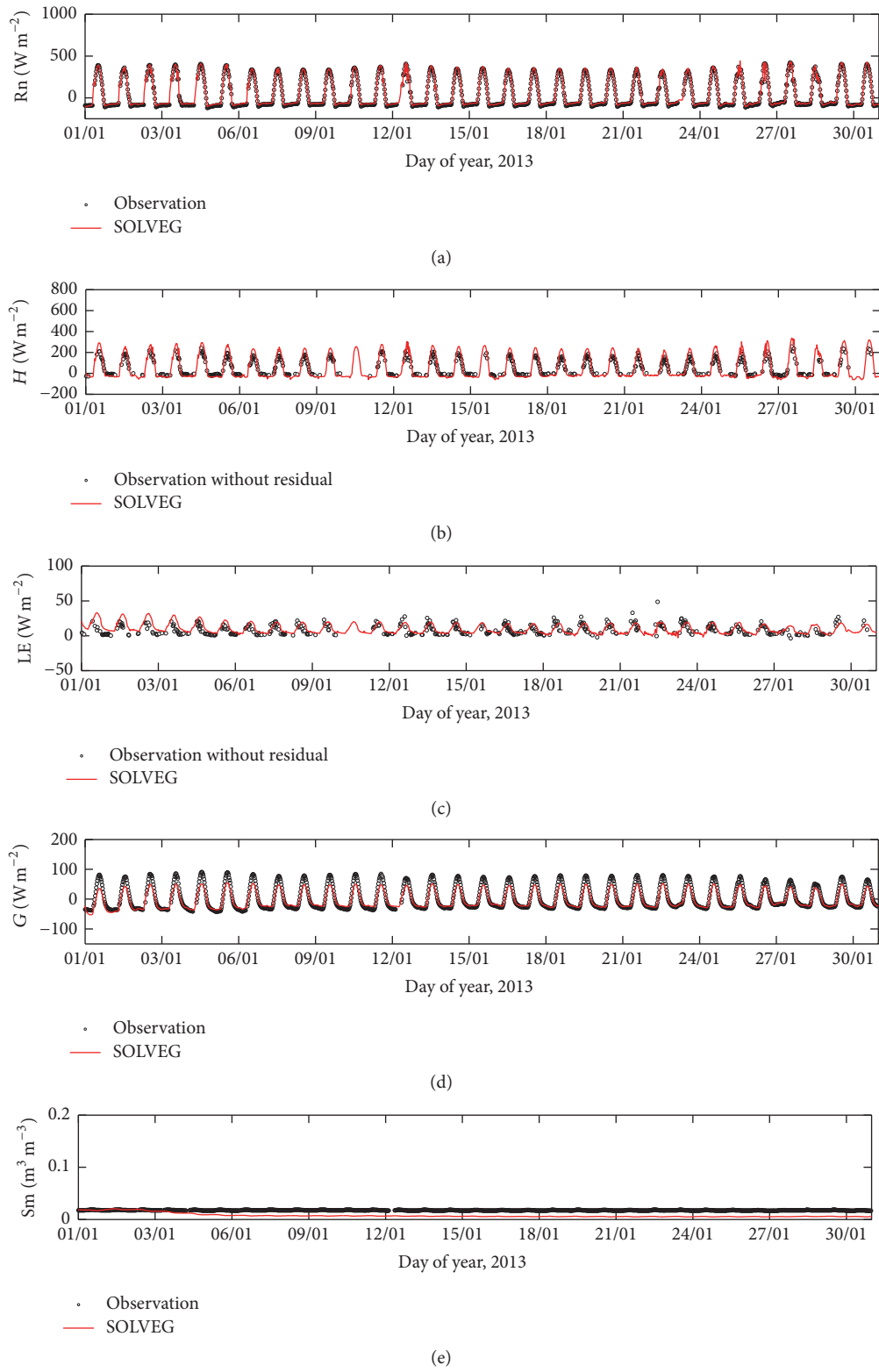
(a)

(b)

(c)

(d)

(e)

FIGURE 2: Temporal changes in (a) net radiation, (b) sensible heat flux, (c) latent heat flux, (d) ground heat flux, and (e) volumetric soil moisture content at a depth of 0.03 m at the study site during the dry period.

TABLE 3: Summary of the statistical comparison of the simulated variables against the observed variables for several performance measures: correlation coefficient R, normalized standard deviation σ, and centred root mean square error (RMSE).

Parameter	R		Normalised std		Centred RMSE	
	Dry period	Wet period	Dry period	Wet period	Dry period	Wet period
Rn	0.99	0.98	0.99	0.96	0.05	0.19
H	0.99	0.94	2.23	2.82	1.25	1.92
Hn	0.91	0.90	1.03	1.41	0.42	0.67
LE	0.63	0.83	0.95	0.13	0.88	0.88
LEn	0.67	0.81	0.35	0.09	0.83	0.90
G	0.99	0.94	0.51	0.95	0.50	0.38
Sm	0.32	0.89	0.60	1.05	1.00	0.50

and is reproduced in the simulation (Figure 2(e)). Similarly, the time series of the simulated and the corrected observed H and LE (with the residual energy) are provided in Figure 3. The maximum daily values of corrected observed H and LE are 413 and 89 W m^{-2}, respectively.

The statistics based on the Taylor Diagram, TD for the period (Figure 4(a)), reveal that the simulated Rn in the dry period generally agree well with the observations, with a small centred root-mean-square error (RMSE) ~ 0.05 and a high correlation coefficient (R) close to 0.99. In addition, Rn shows normalized standard deviation (σ) of ~0.99 very close to the observation (1.00), an indication that the pattern variations are of the right amplitudes (Figure 2(a)). The simulated H has R value of 0.99, with RMSE and σ of 1.25 and 2.23, respectively (Figure 4(a)), indicating a slightly lower model performance compared to the simulation of the net radiation.

The model performance for the latent heat flux is moderate (Figure 2(c)), indicated by values of 0.63, 0.838, and 0.95 for R, RMSE and σ, respectively (Figure 4(a)). Figure 2(d) shows that the strong diurnal variability of ground heat fluxes during the dry period is well reproduced by SOLVEG leading to a high correlation coefficient of 0.99. However, the normalized standard deviations σ (~0.51) indicates a moderate underestimation of the observed variability mostly around noon, whereas the rest of the diurnal variability is well captured. The performance measures for the soil moisture content are R (~0.32), σ (~0.60) and RMSE (~1.00), which indicates a modest performance regarding the simulation of soil moisture.

Figure 3 represents the time series after the residual energy has been included in the observed H and LE. It illustrates that, during the night time, the model simulations tend to overestimate the observed heat fluxes. In addition, the statistics (Figure 4(a)) reveals that the simulated H and LE, now Hn and LEn, show normalised standard deviation (σ) of 1.03 and 0.35, respectively (Figure 4(a)), which suggest that the inclusion of the residual energy in the observed fluxes ((4) and (5)) resulted in an improvement in the simulated Hn, but too little variation for simulated LEn. Furthermore, this led to their underestimation of the noon time values in both variables by the model (Figures 2(b) and 2(c)). This is an indication that the lack of energy closure at the study site during the period could not have been the only reason for the model's overestimation of the observed energy fluxes

(Figures 2(b) and 2(c)). Summary of the statistics of the model evaluation for the dry period is provided in Table 3.

3.2. Wet Period Simulation. Figure 5 depicts the time series of observed and simulated surface energy fluxes and volumetric soil water content during the wet period for selected days from 1 to 26 June, 2013. The model simulations can capture the diurnal patterns of the observed variables quite well for all heat fluxes before the rainfall events. After the rainfall events, the model shows clear limitations regarding the simulation of latent heat flux. During the entire wet period, Rn produces value of σ close to the observation (Figure 4(b)) with small RMSE, which suggests that Rn is simulated well by the model in comparison to the other observations. The modelled H is correlated ($R \sim 0.94$) with the observed values. The daily maximum values for the simulated parameters are 692, 433, 203, and 90 W m^{-2} for the Rn, H, LE, and G, respectively, while those for the observed are 638, 274, 424, and 80 W m^{-2} (Figure 5).

It was observed that a rapid increase in soil moisture after rainfall events on June 6, 10, and 20 (Figure 5(e)) caused a rapid reduction in the amplitudes of the observed H and G (Figures 5(b) and 5(d)). This suggest that the dynamics of the soil temperature is related to the volumetric soil water content, as the variability in the amplitudes shows that the changes in the soil surface temperature, a key parameter in the simulation of H and G, affected the model's performance during the wet period. It is therefore important to recognise that the use of a fixed soil temperature in the model especially during the wet period could result in some uncertainties. At the same time, an increase of the observed positive LE was recorded (Figure 5(c)). High water vapour exchange rate continued for subsequent days after the rainfall events when soil water content was quite sufficient, but the rate gradually declined with drying processes (Figure 5(e)). The decrease in the values of observed H and G with an increase in the observed LE, after the rainfall events (Figure 5(c)), also suggests that net radiative energy is mainly going into latent heat flux compared with sensible heat flux under wet conditions. This situation during the wet period indicates the important role of rainfall, and hence soil moisture in terms of the energy exchange processes in the African Savanna areas.
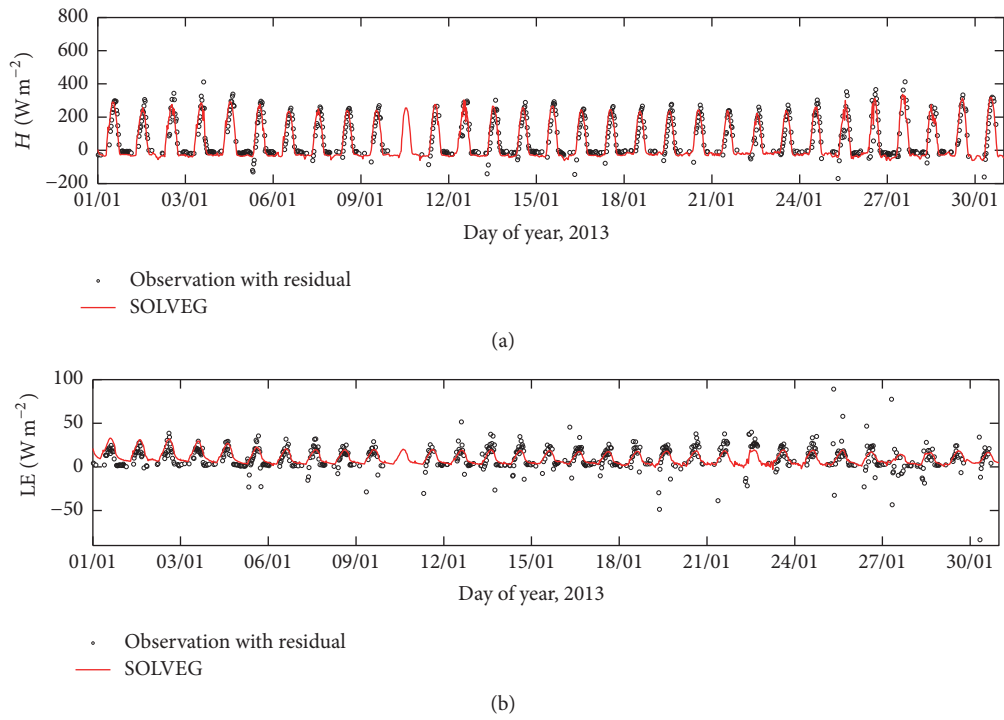
FIGURE 3: Temporal changes in (a) sensible heat flux and (b) latent heat flux, after the residual energy corrections during the dry period.
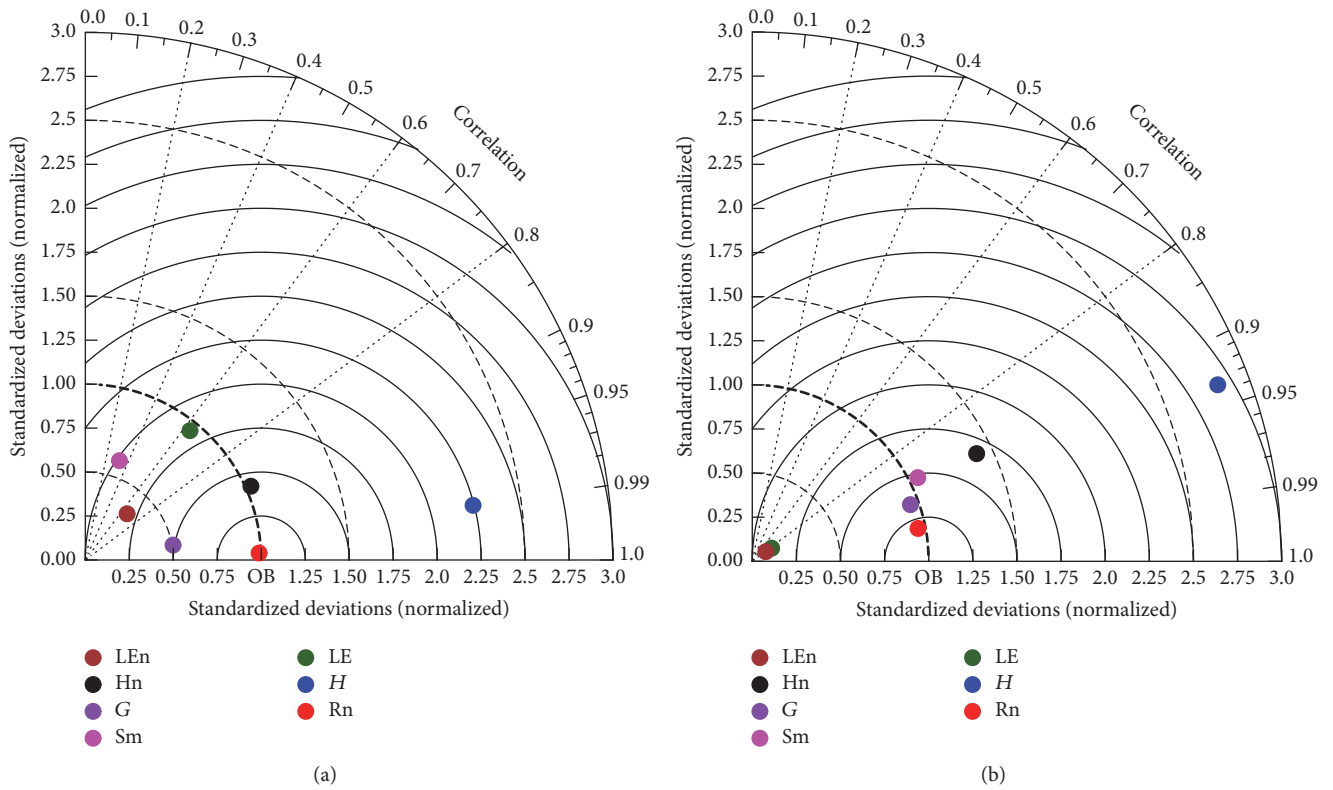

FIGURE 4: Statistical comparison between the simulated and observed variables for (a) the dry period and (b) the wet period at the study site.
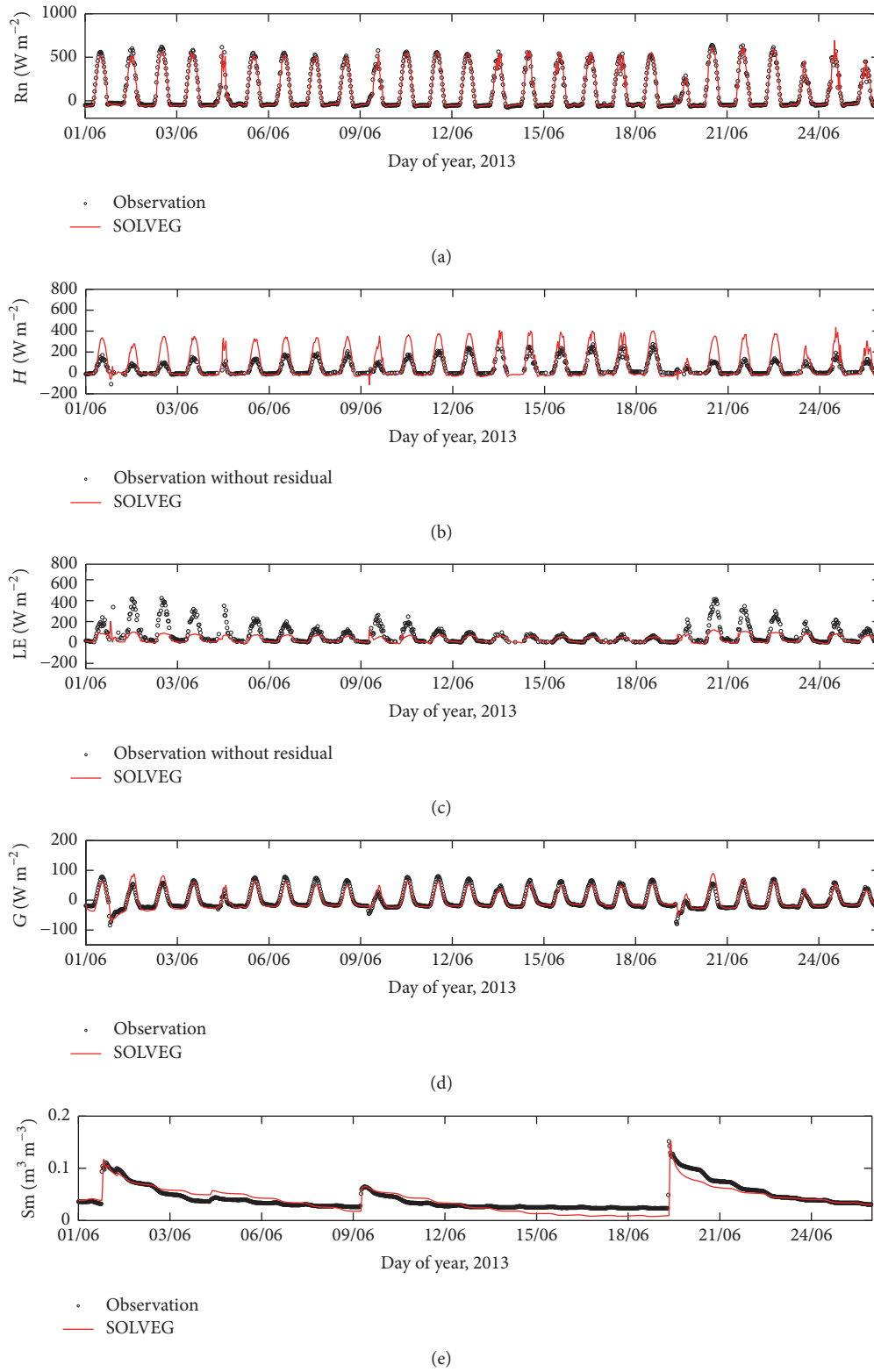
Figure 5: Temporal changes in (a) net radiation, (b) sensible heat flux, (c) latent heat flux, (d) ground heat flux, and (e) soil moisture content at a depth of 0.03 m at the study site during the wet period.
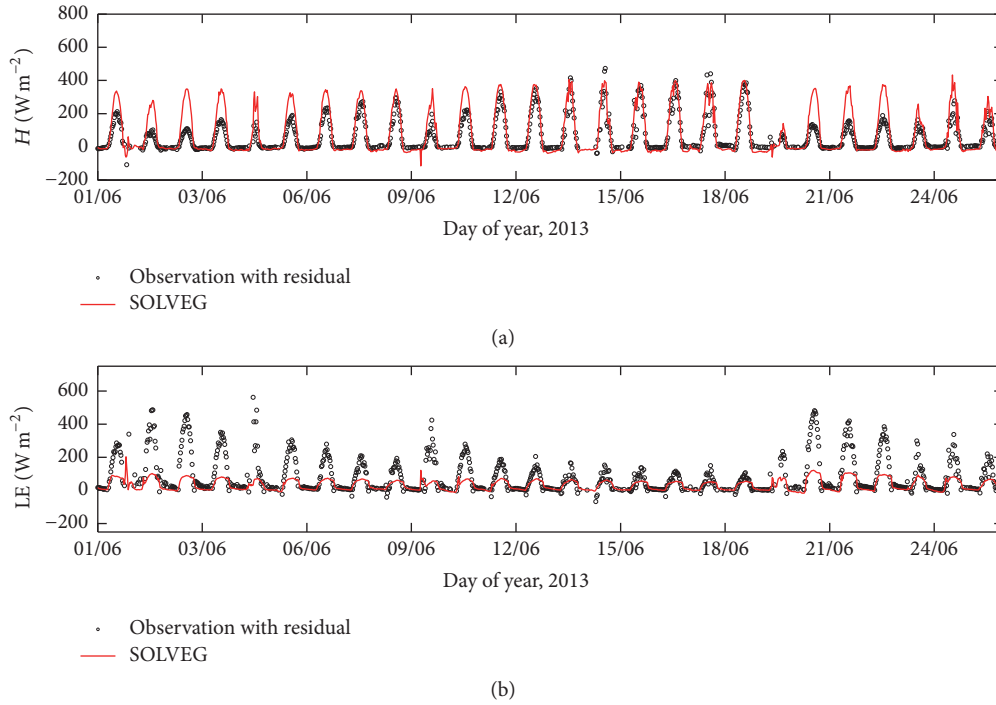
(a)

(b)

FIGURE 6: Temporal changes in (a) sensible heat flux and (b) latent heat flux, after the residual energy corrections during the wet period.

Bagayoko et al. [8] using the Noah-LSM over the region attributed the underestimation of LE by the model in the wet period to the measurement device, as raindrops could accumulate on the lenses of the Krypton Hygrometer used, causing an overestimation of the measured LE. In contrast, the software (TK3) [19], used to process the raw data for the current study, takes care of raindrops and dust particles as part of its quality control measures to prevent the influence of accumulated dust and raindrops on the measurement instruments that can potentially affect the observed H and LE fluxes and hence the model's performance. It was therefore not expected that the dust and raindrops during the selected days in the dry and wet periods over our study site could be contributing factors to the discrepancies in the observed and simulated H and LE.

The statistics show that, before the inclusion of the residual energy, the simulated H and LE produce normalised σ of 2.82 and 0.13, respectively, compared to the observation. However, after the inclusion of the residual energy (Figure 6), these values (now Hn and LEn) are reduced to σ of 1.41 and 0.09, respectively (Figure 4(b)). This again suggests that other reasons besides the lack of energy closure at the site for the selected days during the wet period could be responsible for the model's overestimation and underestimation of observed H and LE, respectively. Summary of the statistics of the model evaluation for the period is also provided in Table 3.

3.3. Uncertainties due to the Energy Balance Closure Problem. The observed energy balance closure for the selected days during the dry and wet periods was estimated at 60 and 68%,

respectively, indicating that a significant part of energy flux cannot be explained by only vertical exchange processes in our study site. Since Land Surface Models close the surface energy budget by definition, it was necessary to address the shortfall in the observed turbulence fluxes (H + LE) for a better comparison with the simulated H and LE. Although the inclusion of the residual energy in the turbulence fluxes reduced the variability in terms of the normalised standard deviation, these were not significant enough to suggest that the lack of energy closure at the site during the study periods is responsible for the model's performance in simulating the turbulence fluxes (H + LE). Again the inability of the model to capture the diurnal patterns of the H and LE after the rainfall events showed that the schemes for evaporation and water adsorption under semiarid conditions need to be investigated further. More sensitivity tests are therefore required to improve the model performance and to understand the processes that lead to the efflux of surface energy in the model.

4. Summary and Conclusions

To understand the surface exchange processes in arid and semiarid environments, numerical simulations of net radiation (R), sensible heat flux (H), latent heat flux (LE), ground heat flux (G), and volumetric soil moisture content (Sm) over a semiarid grassland ecosystem were carried out using a multilayer atmosphere-SOil-VEGetation (SOLVEG) model. The model is unique in including the schemes of evaporation and water adsorption within the dry soil. The schemes for

water movements simulate evaporation even during dry conditions when the soil moisture content reaches the wilting point. The observational data from the Sudanian Savanna region is also unique for validating the model performance in semiarid grassland ecosystem.

We also performed a correction of the H and LE to improve the imbalance of the surface energy budget and to compare the corrected fluxes against the model simulations. The results demonstrated that SOLVEG was able to simulate the energy fluxes, most especially the Rn over the entire investigation period for the selected days in both the dry and wet periods in 2013, indicated in general by small centred root mean square error and high coefficients of correlation (Table 3). However, the results showed a shortcoming of SOLVEG regarding the partitioning of H and LE after rainfall events.

The simulated H and LE in comparison with the observed H and LE (without the residual energy) showed values of normalised standard deviation (σ) of 2.23 and 0.93, respectively, for the dry period, while in the wet period, they were 2.82 and 0.13, respectively. The inclusion of the residual energy in the observed H and LE led to values of the simulated Hn and LEn of σ approximately 1.03 and 0.35 for the dry period and 1.41 and 0.09, respectively, for the wet period. The outcomes of this comparison revealed that differences between the observed and simulated H and LE are not only a result of the lack of energy balance closure observed at the study site for the study periods. In addition, the poor performance of SOLVEG to capture the diurnal patterns of the observed H and LE after rainfall demonstrated the need to further investigate the schemes for evaporation and water adsorption under arid and semiarid conditions. Since the current evaluation period was very short, further model simulations over a longer period (e.g., one year) are necessary to investigate the model performance in more details in order to better understand the processes of surface energy exchanges over the savanna regions in West Africa.

Competing Interests

The authors declare that there is no conflict of interests regarding the publication of this paper.

Acknowledgments

References

[1] M. Williams, A. D. Richardson, M. Reichstein et al., "Improving land surface models with FLUXNET data," *Biogeosciences*, vol. 6, no. 7, pp. 1341–1359, 2009.

[2] J. Ingwersen, K. Steffens, P. Högy et al., "Comparison of Noah simulations with eddy covariance and soil water measurements at a winter wheat stand," *Agricultural and Forest Meteorology*, vol. 151, no. 3, pp. 345–355, 2011.

[3] A. J. Pitman, "The evolution of, and revolution in, land surface schemes designed for climate models," *International Journal of Climatology*, vol. 23, no. 5, pp. 479–510, 2003.

[4] I. C. Prentice, X. Liang, B. E. Medlyn, and Y.-P. Wang, "Reliable, robust and realistic: the three R's of next-generation land-surface modelling," *Atmospheric Chemistry and Physics*, vol. 15, no. 10, pp. 5987–6005, 2015.

[5] E. Rosero, Z.-L. Yang, L. E. Gulden, G.-Y. Niu, and D. J. Gochis, "Evaluating enhanced hydrological representations in Noah LSM over transition zones: implications for model development," *Journal of Hydrometeorology*, vol. 10, no. 3, pp. 600–622, 2009.

[6] T. S. Hogue, L. Bastidas, H. Gupta, S. Sorooshian, K. Mitchell, and W. Emmerich, "Evaluation and transferability of the Noah land surface model in semiarid environments," *Journal of Hydrometeorology*, vol. 6, no. 1, pp. 68–84, 2005.

[7] D. Schüttemeyer, *The Surface Energy Balance Over Drying Semi-arid Terrain in West Africa*, University of Wageningen, Wageningen, The Netherlands, 2005.

[8] F. Bagayoko, S. Yonkeu, and N. C. van de Giesen, "Effect of seasonal dynamics of vegetation cover on land surface models: a case study of NOAH LSM over a savanna farm land in eastern Burkina Faso, West Africa," *Hydrology and Earth System Sciences Discussions*, vol. 3, no. 5, pp. 2757–2788, 2006.

[9] R. Grote, E. Lehmann, C. Brümmer, N. Brüggemann, J. Szarzynski, and H. Kunstmann, "Modelling and observation of biosphere-atmosphere interactions in natural savannah in Burkina Faso, West Africa," *Physics and Chemistry of the Earth*, vol. 34, no. 4-5, pp. 251–260, 2009.

[10] F. Chen and J. Dudhia, "Coupling an advanced land surface-hydrology model with the Penn State-NCAR MM5 modeling system. Part I: model implementation and sensitivity," *Monthly Weather Review*, vol. 129, no. 4, pp. 569–585, 2001.

[11] H. Nagai, "Incorporation of CO_2 exchange processes into a multilayer atmosphere–soil–vegetation model," *Journal of Applied Meteorology*, vol. 44, no. 10, pp. 1574–1592, 2005.

[12] G. Katata, H. Nagai, H. Ueda, N. Agam, and P. R. Berliner, "Development of a land surface model including evaporation and adsorption processes in the soil for the land-air exchange in arid regions," *Journal of Hydrometeorology*, vol. 8, no. 6, pp. 1307–1324, 2007.

[13] J. Bliefernicht, H. Kunstmann, L. Hingerl et al., "Field- and simulation experiments for investigating regional land-atmosphere interactions in West Africa: experimental setup and first results," in *Climate and Land Surface Changes in Hydrology*, E. Boegh, E. Blyth, D. M. Hannah et al., Eds., vol. 359 of *IAHS RedBook Series*, pp. 226–232, IAHS, 2013.

[14] E. Quansah, M. Mauder, A. A. Balogun et al., "Carbon dioxide fluxes from contrasting ecosystems in the Sudanian Savanna in West Africa," *Carbon Balance and Management*, vol. 10, article 1, 2015.

[15] D. Kpongor, *Spatially Explicit Modeling of Sorghum (Sorghum bicolor L) Production on Complex Terrain of a Semi-arid Region of Ghana Using APSIM*, vol. 51, Edited by P. L. G. Vlek, M. Denich, C. Martius, and N. van de Giesen, Cuvillier, Göttingen, Germany, 2007.

[16] J. Ardö, M. Mölder, B. A. El-Tahir, and H. A. M. Elkhidir, "Seasonal variation of carbon fluxes in a sparse savanna in semi arid Sudan," *Carbon Balance and Management*, vol. 3, article no. 7, 2008.

[17] C. Brümmer, H. Papen, R. Wassmann, and N. Brüggemann, "Fluxes of CH_4 and CO_2 from soil and termite mounds in south Sudanian savanna of Burkina Faso (West Africa)," *Global Biogeochemical Cycles*, vol. 23, no. 1, Article ID GB1001, 2009.

[18] B. Ibrahim, J. Polcher, H. Karambiri, and B. Rockel, "Characterization of the rainy season in Burkina Faso and it's representation by regional climate models," *Climate Dynamics*, vol. 39, no. 6, pp. 1287–1302, 2012.

[19] M. Mauder and T. Foken, *Documentation and Instruction Manual of the Eddy-Covariance Software Package TK3*, Arbeitsergebnisse 46, Universität Bayreuth, Abteilung Mikro-Meteorologie, Bayreuth, Germany, 2011.

[20] T. Foken, "The energy balance closure problem: an overview," *Ecological Applications*, vol. 18, no. 6, pp. 1351–1367, 2008.

[21] T. E. Twine, W. P. Kustas, J. M. Norman et al., "Correcting eddy-covariance flux underestimates over a grassland," *Agricultural and Forest Meteorology*, vol. 103, no. 3, pp. 279–300, 2000.

[22] G. Katata, "Improvement of a land surface model for accurate prediction of surface energy and water balances," JAEA-Data/Code 2008-033, Japan Atomic Energy Agency, 2009.

[23] R. D. Jackson, R. J. Reginato, B. A. Kimball, and F. S. Nakayama, "Diurnal soil-water evaporation: comparison of measured and calculated soil-water fluxes," *Soil Science Society of America Proceedings*, vol. 38, no. 6, pp. 861–866, 1974.

[24] S. W. Webb, "A simple extension of two-phase characteristic curves to include the dry region," *Water Resources Research*, vol. 36, no. 6, pp. 1425–1430, 2000.

[25] M. T. van Genuchten, "Closed-form equation for predicting the hydraulic conductivity of unsaturated soils," *Soil Science Society of America Journal*, vol. 44, no. 5, pp. 892–898, 1980.

[26] G. S. Campbell and S. Shiozawa, "Prediction of hydraulic properties of soils using Particle-size distribution and bulk density data," in *Proceedings of the International Workshop on Indirect Methods for Estimating the Hydraulic Properties of Unsaturated Soils*, pp. 317–328, University of California, 1992.

[27] K. E. Taylor, "Summarizing multiple aspects of model performance in a single diagram," *Journal of Geophysical Research Atmospheres*, vol. 106, no. 7, pp. 7183–7192, 2001.